Improving beamforming by optimization of acoustic array microphone positions

Malgoezar, Anwar; Snellen, Mirjam; Sijtsma, Pieter; Simons, Dick

Publication date
2016

Document Version
Final published version

Published in
6th Berlin Beamforming Conference

BeBeC-2016-S5

IMPROVING BEAMFORMING BY OPTIMIZATION OF ACOUSTIC ARRAY MICROPHONE POSITIONS

Anwar Malgoezar[1], Mirjam Snellen[1], Pieter Sijtsma[1,2] and Dick Simons[1]
[1]Delft University of Technology, Faculty of Aerospace Engineering
Kluyverweg 1, 2629 HS, Delft, The Netherlands
[2]PSA3 Advanced AeroAcoustics
Prinses Margrietlaan 13, 8091 AV, Wezep, The Netherlands

Abstract

Assigning proper positions to microphones within arrays is essential in order to reduce or eliminate side- and grating lobes in 2D beamform images. In this paper an objective function is derived providing a measure for the presence of artificial sources. Using the global optimization method Differential Evolution an optimized microphone configuration is obtained by minimization of this objective function. Results show that optimizing the microphone locations can significantly enhance the array performance. In a large part of the scan region surrounding the true source location, no side- or grating lobes are present, meaning that the source can be unambiguously located. From the optimization it is also found that the optimized array configuration shows the microphones distributed at almost constant distance. A linear relation is found which shows that the distance decreases with increasing frequency. This knowledge is important information for the design of an optimal microphone configuration.

1. INTRODUCTION

When applying beamforming for imaging acoustic sources, the resulting image identifies the source locations as areas with high sound levels. However, often high levels are also found at locations with no sound source present. We can divide these spurious sources in two groups: side lobes and grating lobes. Grating lobes have levels equal to that of the actual source position. They result from complete constructive interference. For line arrays, for example, they are the result of having inter-microphone distances larger than half the wavelength of the signal of interest. Side lobes are considered as all other areas in the image with high levels, resulting from partial constructive interference.

Due to the nature of an acoustic microphone array it inherently exhibits the appearance of side lobes in the resulting image after beamforming. There are several ways to reduce the presence of grating lobes and side lobes, one more practical and easier to perform than the other. The impractical choices are to use an infinitesimal small distance between microphones to eliminate grating lobes for all frequencies. The other is the use of an infinite amount of microphones to reduce (but not eliminate) the levels of the side lobes, which in turn requires a microphone array of infinite dimension. Alternatively, weighting can be applied. However, this effectively decreases the array aperture and thus the array resolution. Because we are working with a finite amount of microphones we need to look for other solutions.

One way to eliminate side lobes is to apply dedicated beamforming techniques such as adaptive beamforming[1] and functional beamforming[2–4], or deconvolution methods such as CLEAN-PSF, CLEAN-SC[5] and DAMAS[6–8]. These methods start their deconvolution algorithm with source maps obtained by the well-known sum-and-delay beamforming, or, conventional beamforming. Although deconvolution methods work well in certain situations, the quality of the results depends strongly on the quality of the initial source map.

The other approach is to minimize side lobes through array design. Previous work[9–11] shows that careful selection of the microphone locations and array aperture can reduce side lobe levels.

In this work we focus on optimizing the array configuration. As a first step, an objective function is selected which is a measure for the presence of artificial sources. By minimizing this function an optimal microphone distribution is obtained, providing minimal appearance of side lobes. The unknowns are the microphone positions. In order to allow optimization for the large number of unknowns, use is made of Differential Evolution (DE) as the global optimization method. DE is a variant of the well-known genetic algorithm (GA)[12]. Previous work in the field of geo-acoustics[13] showed promising results using the DE method for global optimization problems. As with GA, also DE has a number of setting parameters that need to be chosen well in order to obtain optimal DE performance, i.e., a high probability of locating the optimum at a minimum number of forward calculations. For the geo-acoustic inversion problem[13] an optimal DE setting was derived. However, for the problem considered in this contribution the number of parameters is much larger, requiring an additional effort to find those values for the DE setting parameters that provide good DE performance also for the application at hand. Given this optimal setting, the optimization is readily extended to other objective functions.

In Section 2 conventional beamforming is explained. Section 3.1 presents the objective function used in this work. In Section 3.2 a short description of DE is given and the DE setting parameters are selected. The results of optimizing the microphone positions are presented in Section 4. Here, the optimized array performance is assessed by beamforming over several configurations and frequencies. Also, a measure for the optimized configuration is presented. Conclusions of the work are given in Section 5.

2. CONVENTIONAL BEAMFORMING

A single microphone provides the acoustic level resulting from all sources. Using multiple microphones, i.e., an acoustic array, allows for imaging also the individual noise sources. The most classical technique for finding the acoustic sources is delay-and-sum beamforming, which we

denote by conventional beamforming. In the next sections both the time domain and frequency domain beamforming methods are explained.

2.1. Time domain beamforming

When a source emits an acoustic signal in space, it is expected that the signal, without obstruction, arrives at the array with a certain time delay due to the distance it must travel. Time domain beamforming uses the delayed signals measured at various positions in space. These positions in our case are the microphones on the array.

By eliminating the delays and summing the signals resulting from all microphones for all potential source locations, a so-called source map is obtained. This process is known as beamforming. The beamformer output signal is given by[14]

$$\frac{1}{N}\sum_{n=1}^{N} w_n p_{n,\text{meas}}\left(t+\Delta t_n\right), \tag{1}$$

where N is the total amount of microphones in the array, n an individual microphone, w_n the weight applied to the signal of microphone n, e.g. correcting for transmission losses, $p_{n,\text{meas}}$ the pressure measured at microphone n and Δt_n the time delay between microphone n and the scan point.

Assuming the source to be an acoustic monopole, the expression for the received signal is

$$\frac{A}{r}\mathrm{e}^{-i\omega(t-\Delta t)}, \tag{2}$$

where Δt is the time delay between the source and receiver, separated by a distance r, and A the pressure amplitude for $r = 1$ m. The exponential containing the time delay, $\mathrm{e}^{i\omega\Delta t}$, is the phase shift at position r of the signal with frequency ω. For obtaining the amplitude of the source from Eq. (1) the weights are selected according to Eq. (2) as

$$w_n = \frac{r_n}{r_0}, \tag{3}$$

where r_0 is chosen to be a reference distance and r_n the distance of the scan point to microphone n. For convenience we select $r_0 = 1$ m.

2.2. Frequency domain beamforming

By going from the time domain to the frequency domain, beamforming can be performed per frequency. From Eq. (1) and Eq. (3) for a single microphone n

$$\frac{r_n}{r_0} p_{n,\text{meas}}\left(t+\Delta t_n\right), \tag{4}$$

we get for the Fourier transform

$$\frac{r_n}{r_0} P_{n,\text{meas}}(\omega)\mathrm{e}^{i\omega\Delta t_n}, \tag{5}$$

with $P_{n,\text{meas}}(\omega)$ the Fourier transform of the measured pressure $p_{n,\text{meas}}(t)$.

We can then beamform similarly as with the time domain

$$\frac{1}{N}\sum_{n=1}^{N}\frac{r_n}{r_0}P_{n,\text{meas}}(\omega)\mathrm{e}^{i\omega\Delta t_n}, \tag{6}$$

for the frequency ω. Where in the time domain we would beamform for all frequencies in one go, in the frequency domain beamforming is done per frequency.

An alternative approach often taken towards frequency domain beamforming, leading to a somewhat different expression, is as follows. We define the measurement vector $\mathbf{P}_{\text{meas}}$, containing the measurements $P_{n,\text{meas}}(\omega)$. The model for our measurements is $P_0(\omega)\mathbf{g}$, with $\mathbf{g}$ the steering vector containing the transfer functions $g_n(\omega)$ for all microphones n. $g_n(\omega)$ is[15]

$$g_n(\omega) = \frac{r_0}{r_n}\mathrm{e}^{-i\omega\Delta t_n}, \tag{7}$$

and $P_0(\omega)$ the source spectrum (to be estimated). We thus have

$$\mathbf{P}_{\text{model}} = P_0(\omega)\mathbf{g}, \tag{8}$$

$P_0(\omega)$ is estimated by minimizing the difference between $\mathbf{P}_{\text{model}}$ and $\mathbf{P}_{\text{meas}}(\omega)$. This can solved in the least-squares sense by minimizing

$$\|\mathbf{P}_{\text{meas}} - P_0(\omega)\mathbf{g}\|^2, \tag{9}$$

for which the solution is[16]

$$\hat{P}_0(\omega) = \frac{\mathbf{g}^*\mathbf{P}_{\text{meas}}}{\mathbf{g}^*\mathbf{g}}. \tag{10}$$

For plane waves Eq. (10) is the same as Eq. (6). However for spherical waves they differ in the normalization. Eq. (10) is used in deriving the aperture function in the next section. It gives an estimate for the source spectrum at a certain point in space. By evaluating Eq. (10) for each potential source location the beamform map is obtained.

3. THE OPTIMIZATION PROBLEM

3.1. The objective function

For the derivation of the objective function the assumption is made that the array is in the far field, such that the distance between the array and the source is large enough to assume the incoming signals to be plane waves. In this case we are in the far field and only interested in the direction of the sound. We can describe the pressure signal as

$$p(\vec{x}_n) = \mathrm{e}^{i\vec{k}\cdot\vec{x}_n}, \tag{11}$$

where $\vec{x}_n$ is the vector connecting the scan point and the n-th microphone and $\vec{k}$ the wave vector which should satisfy

$$\frac{\omega^2}{c^2} - \vec{k}\cdot\vec{k} = 0. \tag{12}$$

In Eq. (12) c is the sound speed.

Considering a source with unit amplitude and wave vector $\vec{k}_0$, the pressure received at the microphones of the array are

$$\mathbf{P}_{\text{meas}} = \begin{bmatrix} e^{\vec{k}_0 \cdot \vec{x}_1} \\ \vdots \\ e^{\vec{k}_0 \cdot \vec{x}_N} \end{bmatrix}. \tag{13}$$

The steering vector towards a scan point in direction $\vec{k}$ is

$$\mathbf{g} = \begin{bmatrix} e^{\vec{k} \cdot \vec{x}_1} \\ \vdots \\ e^{\vec{k} \cdot \vec{x}_N} \end{bmatrix}, \tag{14}$$

where $\vec{k}_0$ and $\vec{k}$ both satisfy Eq. (12) i.e. correspond to the same frequency. We obtain

$$\mathbf{g}^* \mathbf{g} = \left(e^{-i\vec{k} \cdot \vec{x}_1} e^{i\vec{k} \cdot \vec{x}_1} + \cdots + e^{-i\vec{k} \cdot \vec{x}_N} e^{i\vec{k} \cdot \vec{x}_N} \right) = N, \tag{15}$$

and

$$\mathbf{g}^* \mathbf{P}_{\text{meas}} = \left(e^{-i\vec{k} \cdot \vec{x}_1} e^{+i\vec{k}_0 \cdot \vec{x}_1} + \cdots + e^{-i\vec{k} \cdot \vec{x}_N} e^{i\vec{k}_0 \cdot \vec{x}_N} \right), \tag{16}$$

such that Eq. (10) becomes

$$\hat{P}_0(\omega) = \frac{1}{N} \sum_{n=1}^{N} e^{i(\vec{k}_0 - \vec{k}) \cdot \vec{x}_n}. \tag{17}$$

Eq. (17) can be seen as an aperture smoothing function W,

$$W\left(\vec{k}_0 - \vec{k}\right). \tag{18}$$

To eliminate side lobes the aperture function should satisfy

$$W\left(\vec{k}_0 - \vec{k}\right) = \begin{cases} 1 & \text{if } \vec{k} = \vec{k}_0 \\ 0 & \text{if } \vec{k} \neq \vec{k}_0 \end{cases}. \tag{19}$$

Using only a finite number of microphones N makes this impossible.

If we consider plane wave beamforming with a planar microphone array in $z = 0$, we get

$$(\vec{k}_0 - \vec{k}) \cdot \vec{x}_n = (k_{0,x} - k_x) x_n + (k_{0,y} - k_y) y_n, \tag{20}$$

and for the aperture function

$$W(k_x, k_y) = \frac{1}{N} \sum_{n=1}^{N} e^{i\left[(k_{0,x} - k_x) x_n + (k_{0,y} - k_y) y_n\right]}, \tag{21}$$

from where we see that beamforming results are shift-invariant with respect to the wave numbers

k_x and k_y. In other words, an incoming wave with wave numbers $k_x = k_{0,x}$ and $k_y = k_{0,y}$ gives the same results as with $k_x = 0$ and $k_y = 0$, but shifted by $(k_x, k_y) = (k_{0,x}, k_{0,y})$. We can therefore write

$$W(k_x, k_y) = \frac{1}{N} \sum_{n=1}^{N} \mathrm{e}^{-i\left(k_x x_n + k_y y_n\right)}. \tag{22}$$

Now, to minimize side lobes the following objective, or energy, function is defined

$$J(\vec{x_1}, \cdots, \vec{x_N}) = \int_{\Omega} |W(k_x, k_y)|^2 \mathrm{d}k_x \mathrm{d}k_y = \frac{1}{N^2} \iint_{\Omega} \left| \sum_{n=1}^{N} \mathrm{e}^{-i\left(k_x x_n + k_y y_n\right)} \right|^2 \mathrm{d}k_x \mathrm{d}k_y, \tag{23}$$

where J is the function to be minimized, i.e. the aperture function squared, conform Sijtsma[16]. The power of 2 is used for ease of implementation and computational considerations. The domain Ω contains all scan directions of interest. In order to minimize the side lobes, the domain will be chosen such that it includes all scan directions of interest, but excludes the main lobe.

We can rewrite Eq. (23) as

$$\begin{aligned} J(\vec{x_1}, \cdots, \vec{x_N}) = \frac{\pi k}{N^2} \Big(& Nk \left[\sin^2(\phi_{max}) - \sin^2(\phi_{min}) \right] \\ & + 4 \sum_{m=1}^{N-1} \sum_{n=m+1}^{N} \frac{\sin(\phi_{max}) J_1[k \sin(\phi_{max}) d_{mn}] - \sin(\phi_{min}) J_1[k \sin(\phi_{min}) d_{mn}]}{d_{mn}} \Big), \end{aligned} \tag{24}$$

where d_{mn} is the distance between microphone m and n, $k = |\vec{k}|$ and J_1 is the first order Bessel function of the first kind. The derivation of Eq. (24) can be found in the Appendix. The angles ϕ are elevation angles as can be seen in Figure 1; ϕ_{min} and ϕ_{max} determine the domain Ω.

Suitable integration bounds

In order to minimize the side lobes while excluding the main lobe, the integration boundaries ϕ_{min} and ϕ_{max} need to be selected carefully. The problem of beamforming with an array of microphones is somewhat similar to the descriptions of the best focused spot of light that a perfect lens with a circular aperture can make, limited by the diffraction of light. Whereas in optics the lens 'applies' the phase shift, in acoustic beamforming this would be the microphones. We are going to use this analogy to obtain practical choices for ϕ_{min} and ϕ_{max}. Like in optics we expect the signal resulting from beamforming to have the behaviour of a Bessel function. To clarify this, assume an infinite amount of microphones on a circular array with radius R. We

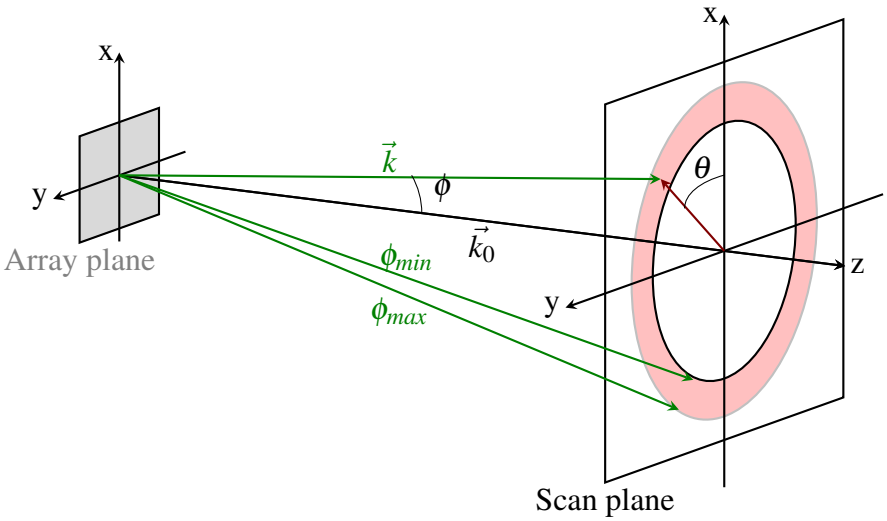

Figure 1: Relation between the wavevector $\vec{k}$, polar angle ϕ and azimuthal angle θ. The area of integration is shown in red. In practice the inner radius will be much closer to the origin.

then have for the aperture function Eq. (22)

$$W(k_x,k_y) \sim \frac{1}{\pi R^2}\iint_{\Omega} \mathrm{e}^{-i\left(k_x x+k_y y\right)}\mathrm{d}x\mathrm{d}y \tag{25}$$

$$= \frac{1}{\pi R^2}\int_0^R\int_0^{2\pi} r\mathrm{e}^{-irk\sin(\phi)}\mathrm{d}\theta\mathrm{d}r \tag{26}$$

$$= \frac{2J_1\left(kR\sin(\phi)\right)}{kR\sin(\phi)}, \tag{27}$$

with $r=\sqrt{x^2+y^2}$ and using similar coordinate transformations and steps as deriving the objective function in the Appendix. Eq. (27) squared is known as the Airy pattern and can be seen in Figure 2. Using this expression we define our lower boundary ϕ_{min} to exclude the main lobe which occurs at the first zero crossing of Eq. (27). For a Bessel function of the first order this corresponds to $J_1(u)=0$, or $u\approx 3.83$. Thus

$$kR\sin(\phi_{min}) = 3.83. \tag{28}$$

For small angles ϕ we find

$$\phi_{min} = 1.22\frac{c}{Df}, \tag{29}$$

with $D=2R$ the diameter of the circular array. Eq. (29) is known as the *Rayleigh criterion* and is known as the angular resolution of an imaging device for the given frequency f.

For the maximum angle ϕ_{max} we select a value based on the desired angular field-of-view (FOV) of 60° or $\phi_{max}=30°$.

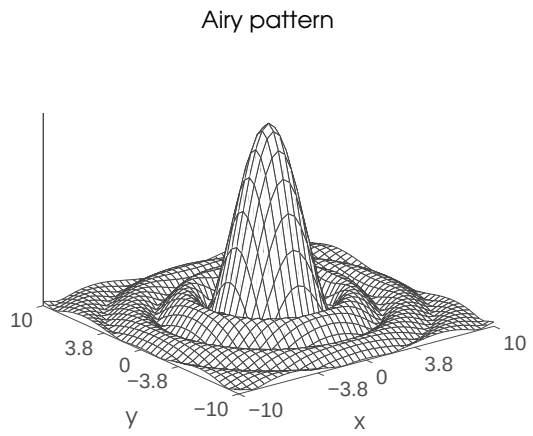

Figure 2: Surface plot of the Airy pattern.

Interpretation of the objective function

In the ideal case, the value of the objective function should yield zero by excluding the origin in the integration. However, due to the nature of an acoustic array, side lobes are inevitable and therefore values of zero for optimized configurations are not feasible. Therefore we consider two exemplary configurations accompanied with a beamformed image of a point source located at the origin. The frequency of the point source is $f = 2000$ Hz with an SPL of 100 dB. The source is positioned in the far field at a distance of 35 m. One configuration exhibits relatively high side lobe levels in the Ω-minimization region while the other has lower levels. The microphone configuration, the corresponding beamformed image and an intersection of the beamform output at $y = 0$ can be seen in Figure 3. The boundaries corresponding to ϕ_{min} and ϕ_{max} are indicated by two concentric circles in the beamform images. Dashed lines indicate these boundaries in the plots showing the intersection. The radii of the circles are, using Eq (29) and a FOV of 60°, 3.68 and 20.21 m. Within this range it is seen that for the configuration corresponding to $J = 43.5$ relatively high side lobe levels are present compared to the configuration of $J = 8.48$. Outside the optimization region, i.e. $r > 20.21$ m, it is seen that the occurrence and levels of the side lobes are of the same order.

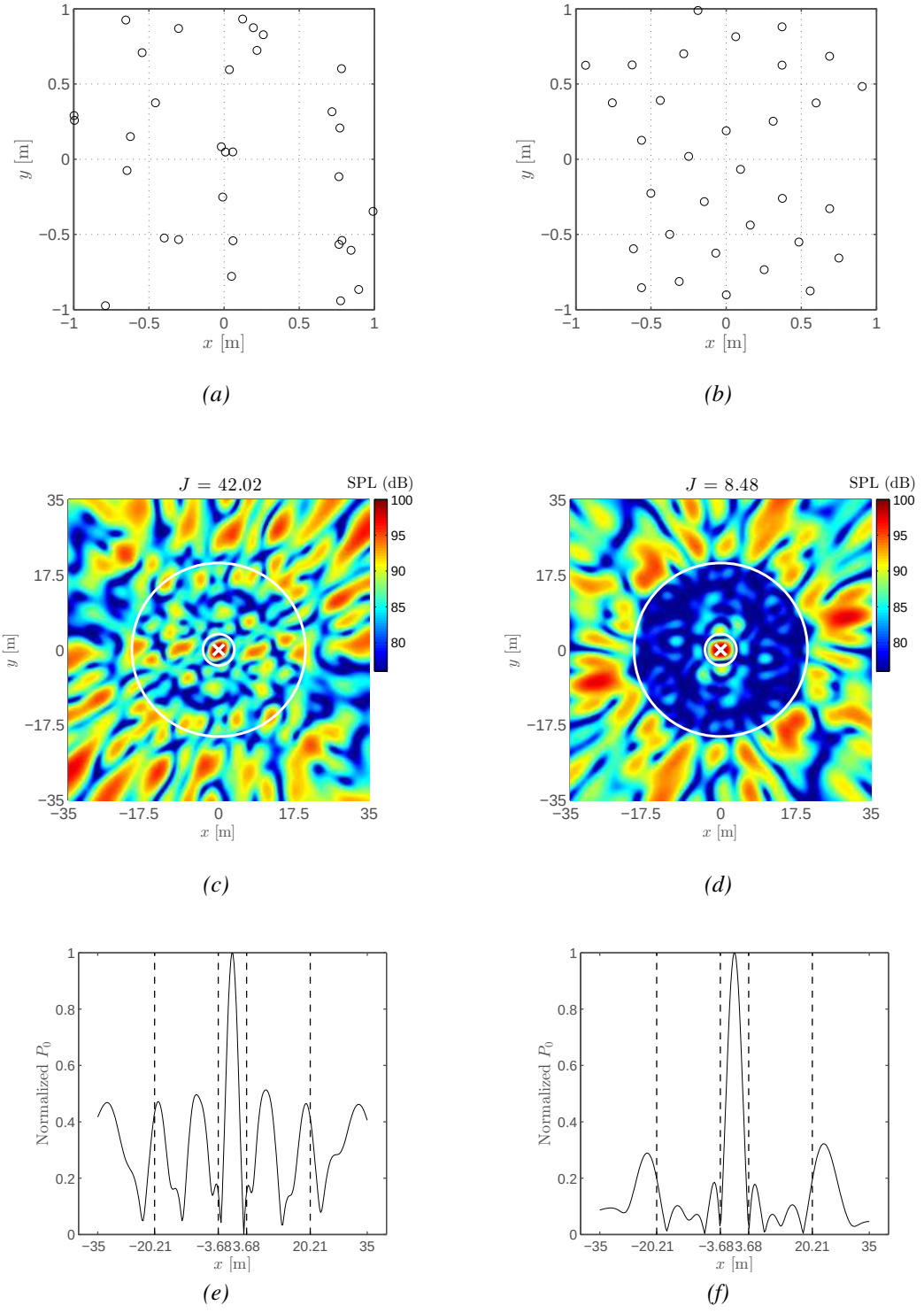

Figure 3: Comparison of side lobes between two configurations with corresponding value of $J = 42.02$ for (a), (c), (e) and $J = 8.48$ for (b), (d), (f).

3.2. The optimization method

Problems related to optimizing an objective function, possibly being nonlinear and non-differentiable over continuous space, can be solved using global optimization methods. In this section we explain the global optimization method differential evolution (DE) used in our problem.

Differential evolution (DE) is a method that optimizes a problem by iteratively trying to improve candidate solutions with regard to a given measure of quality and was introduced by Storn and Price[17, 18]. It can be classified as a metaheuristic method making few or no assumptions about the problem being optimized and can search very large spaces of candidate solutions. However, this metaheuristic method does not guarantee an optimal solution is ever found.

DE is used for multidimensional real-valued functions and does not require the user to calculate the gradient of the problem being optimized, which in turn implies that DE does not require the optimization problem to be differentiable.

DE starts with an initial population of randomly chosen parameter value combinations. The population consists of q members each containing trial values for the unknown parameters. In this problem this equals 64 values corresponding to the (x,y)-coordinates of the 32 microphones. The parameter value combinations are improved each generation over a maximum amount of successive generations N_G. At each generation l, members of the partner population are created from the original population members $\mathbf{m}_{l,i}$ as

$$\mathbf{p}_{l,i} = \mathbf{m}_{l,r_1} + F\left(\mathbf{m}_{l,r_2} - \mathbf{m}_{l,r_3}\right), \tag{30}$$

with $i = 1 \cdots q$. Indices $r_1, r_2, r_3 \in \{1, 2, \cdots, q\}$ are integer, differ from each other and are chosen at random. F is a scalar multiplication factor between 0 and 1. A higher value of F indicates an increased difference between original parameter vector $\mathbf{m}_{l,i}$ and those contained in the partner population $\mathbf{p}_{l,i}$.

The next step is to calculate its descendant $\mathbf{d}_{l,i}$ by applying crossover to $\mathbf{m}_{l,i}$ and $\mathbf{p}_{l,i}$ with a probability p_c. For each parameter j of $\mathbf{d}_{l,i}$ we get

$$d_{l,ij} = \begin{cases} p_{l,ij} & \text{if } [\mathscr{U}(0,1)]_j \leq p_c \\ m_{l,ij} & \text{if } [\mathscr{U}(0,1)]_j > p_c \end{cases}, \tag{31}$$

with $[\mathscr{U}(0,1)]_j$ the j-th evaluation of a uniform distribution with values between 0 and 1. Setting the value of p_c high means that more values are replaced by those of the partner population, while a low value of p_c results in generations that differ only slightly regardless of the value of F.

To create the new generation $l+1$ from the previous generation l, the member $\mathbf{m}_{l,i}$ is replaced by $\mathbf{d}_{l,i}$ only if it yields a smaller value for the objective function

$$\mathbf{m}_{l+1,i} = \begin{cases} \mathbf{d}_{l,i} & \text{if } J(\mathbf{d}_{l,i}) < J(\mathbf{m}_{l,i}) \\ \mathbf{m}_{l,i} & \text{if } J(\mathbf{d}_{l,i}) \geq J(\mathbf{m}_{l,i}) \end{cases}. \tag{32}$$

Doing this for all members i in the population we obtain the next generation $l+1$. This process is repeated for N_G generations.

The so-called setting parameters for DE are

- Population size q,
- Multiplication factor F,
- Crossover probability p_c,
- Number of generations N_G.

These settings which are problem specific must be selected to maximize the probability to locate the global optimum. Next we will try to find the optimal settings.

Finding the optimal settings: number of forward generations and population size

As it is not known beforehand for which combination of setting parameters DE performs best, several tests are carried out to determine the number of generations, population size, multiplication factor and crossover probability.

First the optimal setting for the amount of generations and population size are determined. Hereafter the multiplication factor and crossover probability are selected.

To determine the optimal value for the amount of generations and population sizes, the multiplication factor and crossover probability were set to $F = 0.7$ and $p_c = 0.6$ in accordance with Snellen[13] for the same DE implementation.

A Monte Carlo simulation is performed for population sizes q of 64, 96 and 128, where for each setting 10 independent DE runs are carried out. The result of the energy as a function of generation for the various runs for each population size can be seen in Figure 4. A large variation at 4000 generations can be seen for all population sizes. At 4000 generations the larger population size, $q = 128$, does not outperform $q = 64$. Eight out of the ten runs for $q = 128$ have an energy value between 16 and 18, while for $q = 64$ at least half of the ten runs have a value below 16. To further compare between the different population sizes we look at the amount of forward calculations qN_G. For the three figures in Figure 4 the vertical dashed line indicates the generation for which the number of forward calculations amounts to 256000.

From this it can be seen that a value for $q = 128$ does not on average produce lower values for the energy. This motivates us to use a population size of $q = 64$. While the variation is slightly larger for $q = 64$, the chance to arrive at a lower value for the energy is significantly larger. The same holds when comparing to $q = 96$. Although no full convergence has yet been achieved for $q = 64$ at 4000 generations, we will not increase the amount of generations due to computational constraints. To this end we set the amount of generations to $N_G = 4000$ with a population size of $q = 64$.

Finding the optimal settings: multiplication factor and crossover probability

Having decided on the value for the population size and the amount of generations, two settings remain to be determined. In order to find suitable values for the multiplication factor F and cross over probability p_c, the DE performance is assessed for values for p_c between 0.2 and 1 and F between 0 and 1 with steps of 0.1. For each combination 10 independent runs are done and the average value for the energy value J is determined. The results are shown in Figure 5. From Figure 5 low values of the energy can be seen in the region for $p_c = 0.9$ and $F = 0.2$ to $F = 0.8$. Based on this figure, the best combination to use for DE is found as $p_c = 0.9$ and $F = 0.5$.

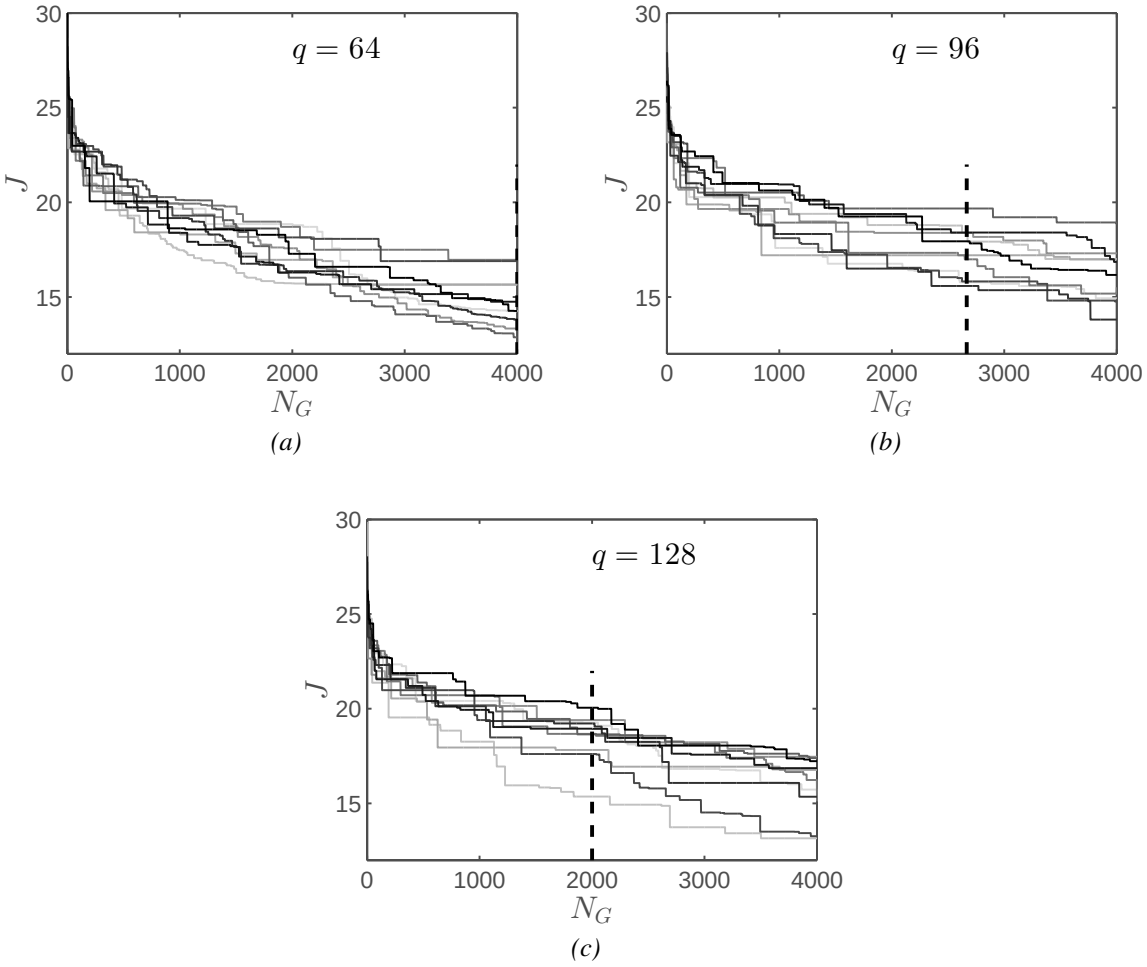

Figure 4: The value of the objective function J as a function of the amount of generations N_G for 10 independent runs with $F = 0.7$, $p_c = 0.6$ for (a) $q = 64$, (b) $q = 96$ and (c) $q = 128$.

4. RESULTS

Optimizing the objective function J of Eq. (24) resulted in various microphone array configurations having low energy values. In Figure 6 several configurations are shown at various stages of an optimization run.

First it can be seen that the configuration for generation 333 becomes more compact compared to the initial configuration by having some microphones closer together. This results in an energy decrease of $J = 23.57$ to $J = 15.86$. From generation 333 and on it can be seen that, while roughly retaining the dimensions of the compact microphone geometry, the microphone positions get more evenly distributed within this geometry, which roughly resembles a circular disc. We can see this happen from generation 333 to 666 with a decrease of $J = 15.86$ to $J = 9.6$. While the configuration at generation 666 and 1500 are very similar, an additional significant decrease of energy can be achieved by going from $J = 9.6$ to $J = 3.96$ by DE through slightly

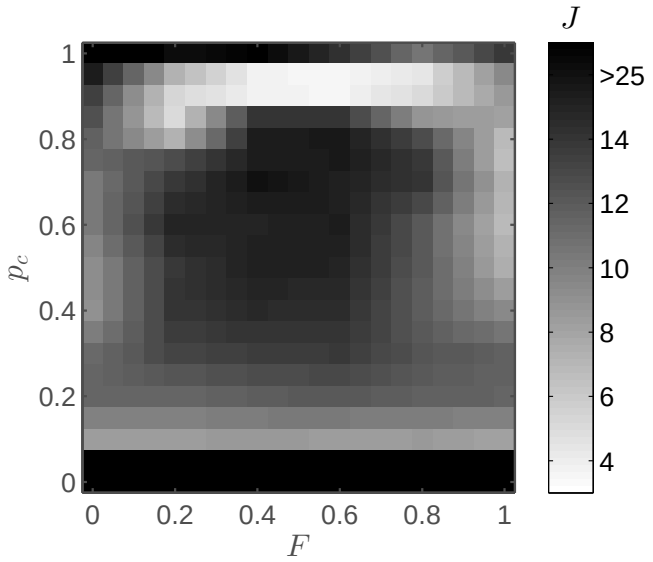

Figure 5: Map of the energy J as a function of p_c and F for $q = 64$ and $N_G = 4000$.

adjusting the microphones and achieving an even more regular pattern. This indicates that the minimum energy corresponds to a specific distance between a microphone and its neighbours. Figure 7 shows the histogram of all distances between the microphones and their closest neighbour for the array configurations of Figure 6. From these histograms it can be seen that towards the final generation these distances tend to fall within the range of 0.16 to 0.28 m. The histograms confirm the formation of a more compact configuration as the variance of the distance decreases, as well as the mean.

4.1. Beamforming with the ideal configuration

For the results presented in the previous section, the frequency selected for optimization was 2000 Hz. Beamforming using the optimized microphone configuration should result in side lobes that are significantly reduced in the optimization region defined in Section 3.1. To demonstrate this and to investigate how the beamforming behaviour is for other frequencies we will beamform for three different frequencies, i.e. lower than 2000 Hz, equal to 2000 Hz and larger than 2000 Hz using the optimal configuration obtained in the previous section. To do this a 100 dB monopole sound source is simulated at the origin at a distance of 35 m. The result of beamforming is shown in Figure 8 for the frequencies 1500, 2000 and 3000 Hz, where the white circles indicate the optimization boundaries corresponding to ϕ_{min} and ϕ_{max}. We can see in Figure 8b that beamforming at the frequency for which the array was optimized (2000 Hz) results in a source map with no side lobes visible in the region of interest and side lobes which are above 80 dB, residing just outside the outer boundary. The main lobe resides just inside the inner boundary indicating that the optimum microphone configuration provides an aperture close to the array diameter. This is confirmed by Figure 6d. We can conclude that beamforming at the frequency for which the microphone configuration was optimized results in side lobes being reduced for the directions of interest.

For the lower frequency (1500 Hz) see Figure 8a, we see that the inner boundary lies inside

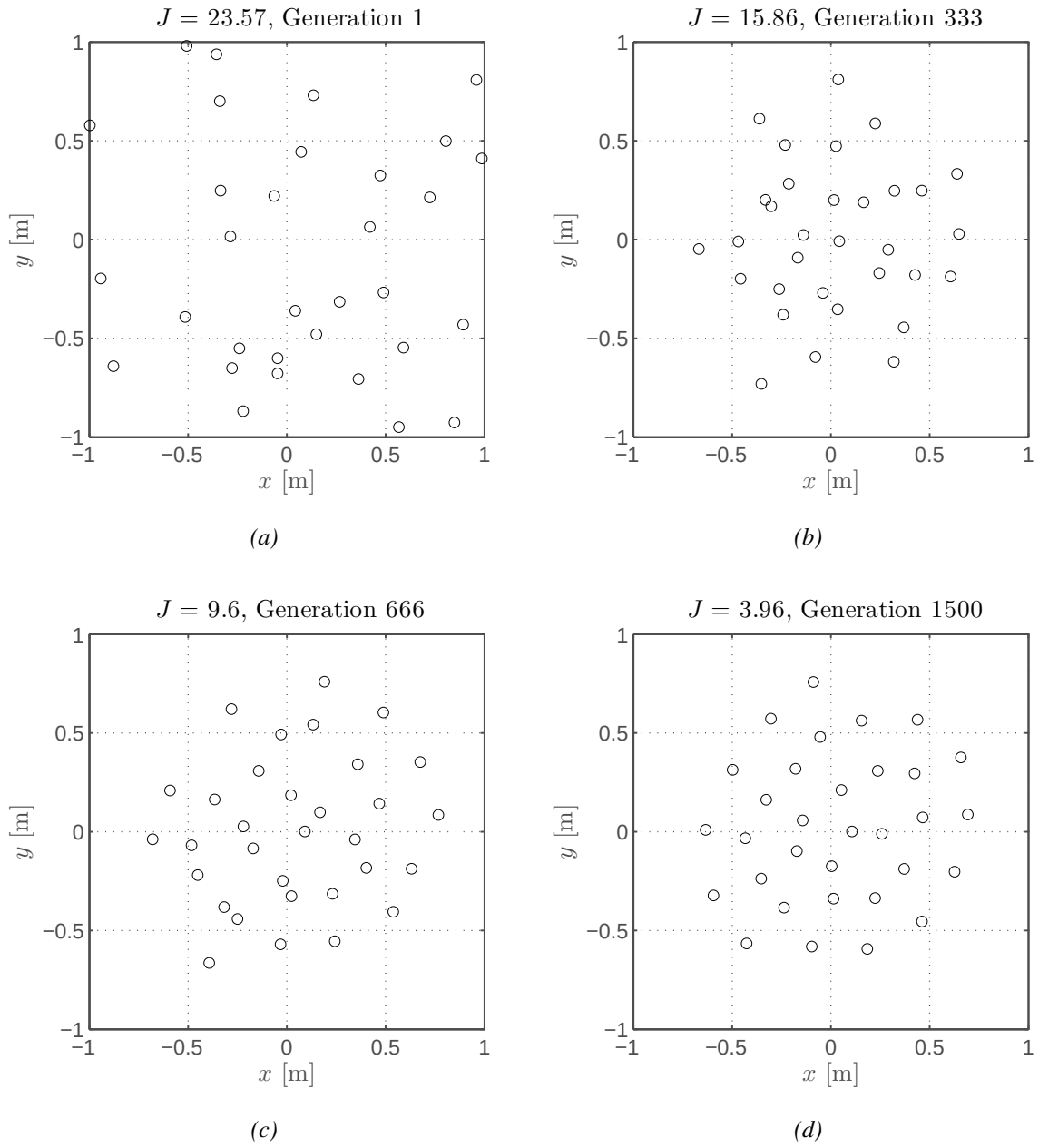

Figure 6: Microphone configurations obtained using $F = 0.2$ and $p_c = 0.8$ for several values of J (a) $J = 23.57$, (b) $J = 15.86$, (c) $J = 9.6$ and (d) $J = 3.96$.

the main lobe. This is expected according to Eq. (29) indicating that lower frequencies result in a wider main lobe while a higher frequencies result in a smaller main lobe. The latter is seen in Figure 8c. Considering the performance of the optimized array at ϕ_{max} Figure 8a indicates for lower frequencies good performance for the FOV of interest but also for larger values of ϕ. In contrast, for higher frequencies the FOV is reduced as side lobes start to appear for values of ϕ smaller than ϕ_{max}.

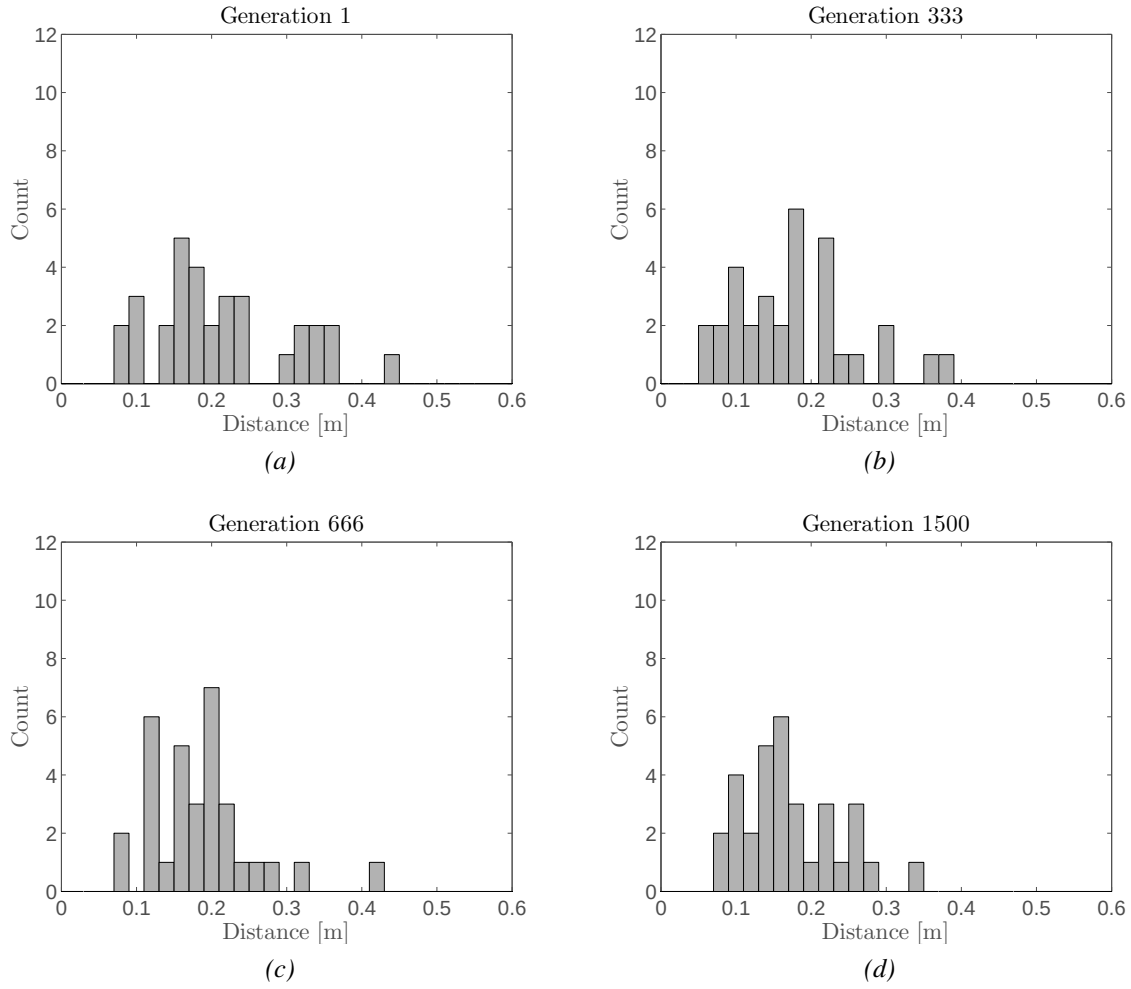

Figure 7: Histograms of the closest-neighbour-distances of the corresponding configurations in Figure 6, (a) $J = 23.57$, (b) $J = 15.86$, (c) $J = 9.6$ and (d) $J = 3.96$.

4.2. Minimum side lobe array design

As a next step the optimization was carried out for frequencies from 1000 Hz to 10000 Hz in 1000 Hz steps. Figure 9 shows the optimized arrays for 2000, 4000 and 6000 Hz, respectively. It can be seen that the separation distance between microphones gets smaller for higher frequencies.

We can also see the energy J getting larger for higher frequencies. This is due to including part of the main lobe. The main lobe size is selected by the lower bound according to Eq. (29). The angle ϕ_{min} will correspond to the main lobe only if the full size of the array, D, is used. Microphone distributions that span only a part of the array, such as seen in Figure 9, will result in larger main lobes. Inclusion of the main lobe will result in a microphone configuration optimized as a compromise between minimum side lobes and small main beamwidth. This is exemplified in Figure 10 and explains why for $f = 4000$ Hz and $f = 8000$ Hz the configuration is not as compact as it could be. An outlier or two for the microphones or a not-as-compact

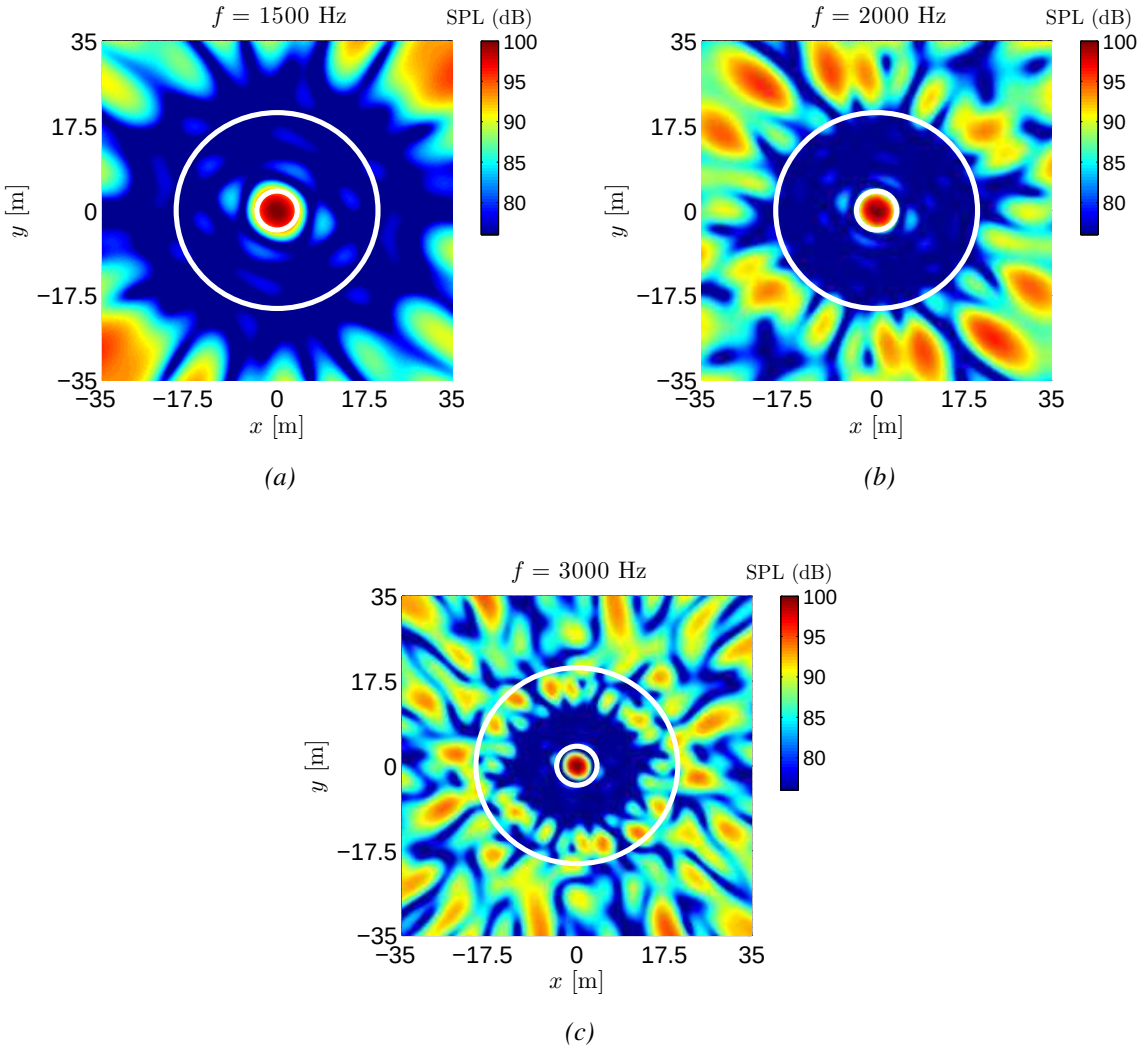

Figure 8: Beamforming with the microphone configuration given in Figure 6d for a simulated source signal at the origin at frequency (a) $f = 1500$ Hz, (b) $f = 2000$ Hz and (c) $f = 3000$ Hz.

configuration can somewhat restrict the further increase of the main lobe width.

Figure 11 shows the histograms for the configurations seen in Figure 9 for the closest-neighbour-distances. Also from the histograms it is clear that the mean of distances decreases with increasing frequency.

To illustrate this more explicitly Figure 12 presents the relation between the *mean* of the closest neighbour distance versus the frequency and wavelength. An approximate linear relation between the distance and the wavelength can be seen. A least squares linear fit for the mean values results in

$$d = 1.38\lambda, \tag{33}$$

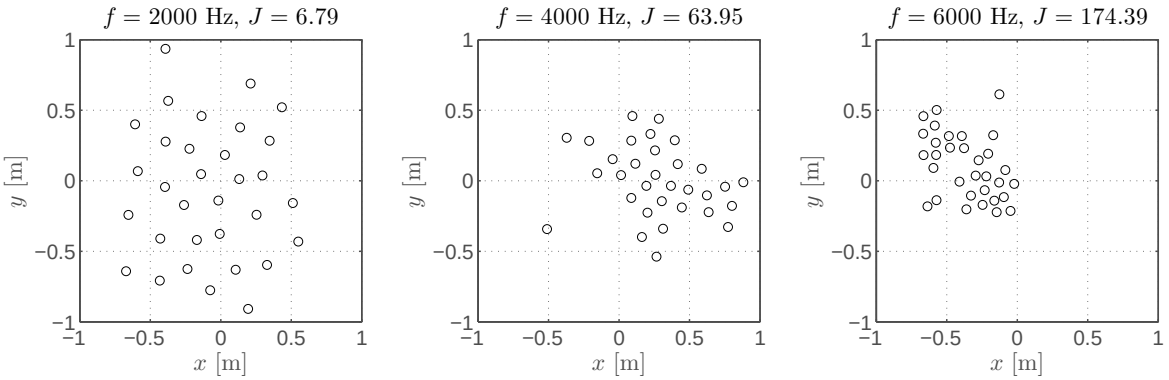

Figure 9: Microphone configurations after optimization for frequencies (a) $f = 2000$ Hz, (b) $f = 4000$ Hz and (c) $f = 6000$ Hz.

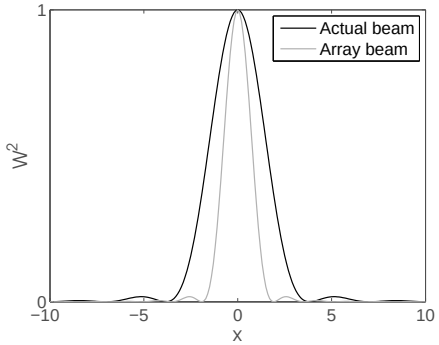

Figure 10: Cross-section of Figure 2 through (0,0) of Airy pattern for the maximum array aperture (array beam) and aperture typically encountered during the optimization (actual beam). Actual beams are always larger or equal to the array beam.

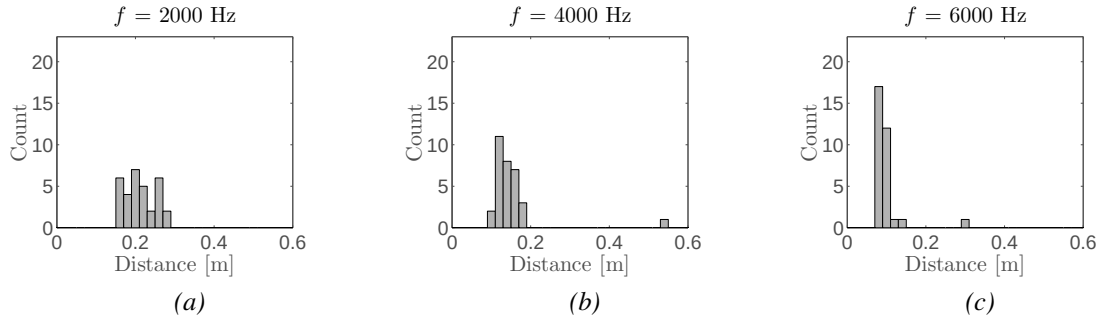

Figure 11: Histograms of closest-neighbour-distance of (a) $f = 2000$ Hz, (b) $f = 4000$ Hz and (c) $f = 6000$ Hz.

for the relation between the closest-neighbour distance d and the wavelength λ, a practical

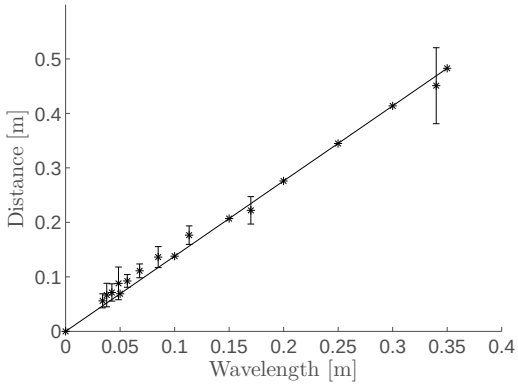

Figure 12: Relation between the closest-neighbour-distance versus the wavelength.

formula which can help in array design.

In order to assess whether the relation found in Eq. (33) can be used to design a microphone configuration, a configuration is constructed by having as many neighbours as possible to have this particular distance.

The configuration was made as a hexagonal pattern by setting three microphones at the vertices of an equilateral triangle and extending this pattern from the origin, ending at the amount of 32. The edges of the equilateral triangle correspond to the closest-neighbour distance. The result can be seen in Figure 13a. The distance was set according to Eq. (33) to $d = 0.2346$ m at the optimization frequency of 2000 Hz. This configuration is such that maximally 6 and at minimum 2 neighbours are at this situated distance. This configuration results in an energy value of

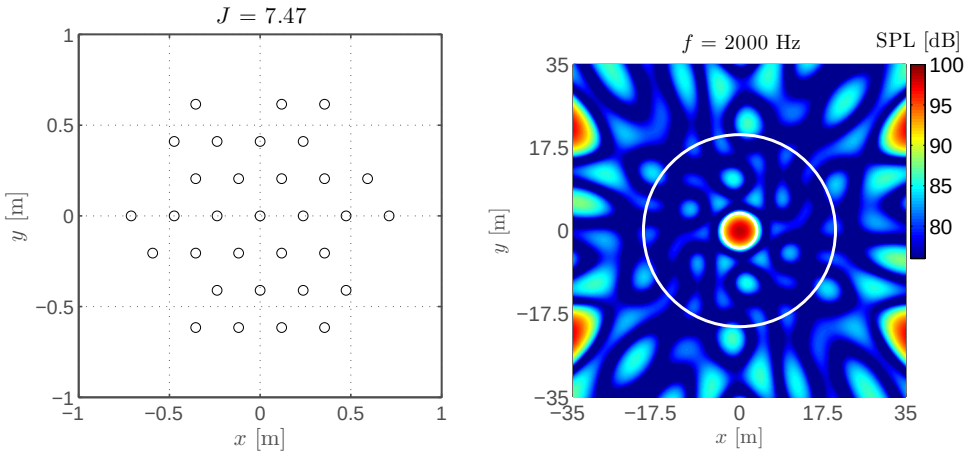

(a) *(b)*

Figure 13: (a) A hexagonal configuration created using the relation in Eq. (33) *and (b) a corresponding beamform image using the configuration.*

$J = 7.47$, which is a low value relative to a random configuration and comparable to the value obtained in the full inversion, see Figure 9a. As a further illustration of the performance of the

configuration seen in Figure 13a the corresponding beamform image is shown in Figure 13b. Good performance with low side lobe levels is seen. However, due to the regular pattern of the hexagonal configuration, side lobes are now visible inside the optimization region. This indicates the need for small deviations for the fixed differences.

5. CONCLUSIONS

In this paper we present a method for optimizing the microphone configurations. The objective function is selected such that it provides a measure for the presence of side- and grating lobes. Minimization of this objective function provides microphone locations, such that no side- and grating lobes are present in a scan region of interest. This region corresponds to the full azimuth and elevation angles ϕ_{min} and ϕ_{max}. The angle ϕ_{min} corresponds to the width of the main lobe, whereas ϕ_{max} corresponds to the maximum elevation angle of interest. For this research, a value of 30 degrees was selected. Low values of the objective function indicates hardly any grating and side lobes present in the region of interest.

For finding the minimum of the objective function use is made of the differential evolution (DE) optimization method. An optimal setting for DE was selected to maximize the probabilities of locating the optimal solution at a minimum number of forward calculations. Optimized array configurations were found using DE which confirmed the desired performance, i.e. low side lobes inside the region of interest.

It is found that the optimized array configuration shows a regular behaviour with the microphones distributed at almost constant distances. From inversions for different frequencies it is found that these distances decrease with frequency and show almost linear behaviour with wavelength. Arrays with microphones positioned based on this linear behaviour show improved performance compared to a random array. Still, the regular pattern gives rise to side lobes that are not present for the microphone configuration obtained through the DE optimization. This indicates the need for small variations of the microphone distances around the distance prescribed by the linear fit.

References

[1] X. Huang, L. Bai, I. Vinogradov, and E. Peers, "Adaptive beamforming for array signal processing in aeroacoustic measurements," *The Journal of the Acoustical Society of America*, vol. 131, no. 3, pp. 2152–2161, 2012.

[2] R. P. Dougherty, "Functional Beamforming," in *Berlin Beamforming Conference 2014-1*, 2014.

[3] R. P. Dougherty, "Functional Beamforming for Aeroacoustic Source Distributions," *AIAA paper*, vol. 3066, June 2014.

[4] R. Merino-Martinez, M. Snellen, and D. G. Simons, "Functional Beamforming Applied to Imaging of Fly-Over Noise on Landing Aircraft," *Submitted to the Journal of Aircraft*.

[5] P. Sijtsma, "CLEAN based on spatial source coherence," *International journal of aeroacoustics*, vol. 6, no. 4, pp. 357–374, 2007.

[6] R. P. Dougherty, "Extensions of DAMAS and Benefits and Limitations of Deconvolution in Beamforming," *AIAA paper*, vol. 2961, no. 11, 2005.

[7] T. F. Brooks and W. M. Humphreys, "A deconvolution approach for the mapping of acoustic sources (DAMAS) determined from phased microphone arrays," *Journal of Sound and Vibration*, vol. 294, no. 4, pp. 856–879, 2006.

[8] T. F. Brooks and W. M. Humphreys, "Extension of DAMAS phased array processing for spatial coherence determination (DAMAS-C)," *AIAA paper*, vol. 2654, 2006.

[9] R. P. Dougherty, "Spiral-shaped array for broadband imaging," Nov. 17 1998. US Patent 5,838,284.

[10] J. R. Underbrink, "Aeroacoustic phased array testing in low speed wind tunnels," in *Aeroacoustic measurements*, pp. 98–217, Springer, 2002.

[11] E. J. Arcondoulis, C. J. Doolan, A. C. Zander, and L. A. Brooks, "Design and calibration of a small aeroacoustic beamformer," in *International Congress on Acoustics (ICA)(20th: 2010: Sydney, New South Wales)*, 2010.

[12] D. Simons and M. Snellen, "Multi-frequency matched-field inversion of benchmark data using a genetic algorithm," *Journal of Computational Acoustics*, vol. 6, no. 01&02, pp. 135–150, 1998.

[13] M. Snellen and D. G. Simons, "An Assessment of the Performance of Global Optimization Methods for GEO-Acoustic Inversion," *Journal of Computational Acoustics*, vol. 16, no. 02, pp. 199–223, 2008.

[14] G. Zechel, A. Zeibig, and M. Beitelschmidt, "Time-domain beamforming on moving objects with known trajectories," in *Berlin Beamforming Conference 2010-12*, 2010.

[15] E. Sarradj, "Three-dimensional acoustic source mapping with different beamforming steering vector formulations," *Advances in Acoustics and Vibration*, vol. 2012, 2012.

[16] P. Sijtsma, "Experimental techniques for identification and characterisation of noise sources," tech. rep., National Aerospace Laboratory NLR, 2004.

[17] R. Storn, "On the usage of differential evolution for function optimization," in *Fuzzy Information Processing Society, 1996. NAFIPS., Biennial Conference of the North American*, pp. 519–523, IEEE, 1996.

[18] R. Storn and K. Price, "Differential evolution–a simple and efficient heuristic for global optimization over continuous spaces," *Journal of global optimization*, vol. 11, no. 4, pp. 341–359, 1997.

[19] M. Abramowitz and I. A. Stegun, *Handbook of mathematical functions: with formulas, graphs, and mathematical tables*. No. 55, Courier Corporation, 1964.

A. The objective function

The integrand of Eq. (23) can be written as

$$\begin{aligned}\left|\sum_{n=1}^{N} \mathrm{e}^{-i\left(k_x x_n + k_y y_n\right)}\right|^2 &= \sum_{m=1}^{N}\sum_{n=1}^{N} \mathrm{e}^{-i\left(k_x x_m + k_y y_m\right)} \mathrm{e}^{i\left(k_x x_n + k_y y_n\right)} \\ &= \sum_{m=1}^{N}\sum_{n=1}^{N} \mathrm{e}^{-i\left[k_x (x_m - x_n) + k_y (y_m - y_n)\right]}.\end{aligned} \tag{34}$$

It is convenient to transform the integration to spherical coordinates using

$$\begin{aligned}k_x &= k\cos(\theta)\sin(\phi) \\ k_y &= k\sin(\theta)\sin(\phi)\end{aligned}, \tag{35}$$

where the relation can be seen in Figure 1. The change in coordinates (k_x, k_y) to (θ, ϕ) requires the change of 'surface' element $\mathrm{d}k_x\mathrm{d}k_x$ to $\mathrm{d}\theta\mathrm{d}\phi$. We can get this from the Jacobian using

$$\mathbf{J} = \begin{bmatrix} \frac{\partial k_x}{\partial \theta} & \frac{\partial k_x}{\partial \phi} \\ \frac{\partial k_y}{\partial \theta} & \frac{\partial k_y}{\partial \phi} \end{bmatrix} = \begin{bmatrix} k\sin(\theta)\sin(\phi) & -k\cos(\theta)\cos(\phi) \\ -k\cos(\theta)\sin(\phi) & -k\sin(\theta)\cos(\phi) \end{bmatrix}, \tag{36}$$

and the change in surface element for the integral according to

$$\mathrm{d}k_x\mathrm{d}k_y = |\det(\mathbf{J})|\,\mathrm{d}\theta\mathrm{d}\phi = k^2\cos(\phi)\sin(\phi)\mathrm{d}\theta\mathrm{d}\phi \tag{37}$$

Using Eq. (34) and the coordinate transformation given by Eqs. (35), Eq. (23) becomes

$$J(\vec{x_1}, \cdots, \vec{x_N}) = \frac{1}{N^2}\sum_{m=1}^{N}\sum_{n=1}^{N}\int_{\phi_{min}}^{\phi_{max}}\int_{0}^{2\pi} k^2\cos(\phi)\sin(\phi)\mathrm{e}^{-ik\sin(\phi)[(x_m - x_n)\cos(\theta) + (y_m - y_n)\sin(\theta)]}\mathrm{d}\theta\mathrm{d}\phi. \tag{38}$$

Integration takes place over all angles, $0 \leq \theta \leq 2\pi$, this means that the addition of *any* constant angle β will not change the result of the integration, i.e.

$$\int_{0}^{2\pi} f(\theta)\,\mathrm{d}\theta = \int_{0}^{2\pi} f(\theta + \beta)\,\mathrm{d}\theta. \tag{39}$$

Applying this to Eq. (38) results in

$$J(\vec{x_1}, \cdots, \vec{x_N}) = \frac{1}{N^2}\sum_{m=1}^{N}\sum_{n=1}^{N}\int_{\phi_{min}}^{\phi_{max}}\int_{0}^{2\pi} k^2\cos(\phi)\sin(\phi)\mathrm{e}^{-ik\sin(\phi)[(x_m - x_n)\cos(\theta+\beta) + (y_m - y_n)\sin(\theta+\beta)]}\mathrm{d}\theta\mathrm{d}\phi. \tag{40}$$

To obtain a solution we will use for the constant angle β

$$\tan(\beta) = \frac{y_m - y_n}{x_m - x_n}. \tag{41}$$

In Figure 14 we can see the relation between the angle β and the distance d_{mn} between two

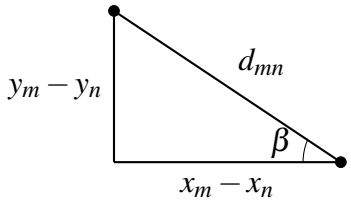

Figure 14: Relation between the angle φ and the sides of the triangle.

microphones n and m. From this figure we get

$$\begin{aligned} x_m - x_n &= d_{mn}\cos(\beta) \\ y_m - y_n &= d_{mn}\sin(\beta), \end{aligned} \tag{42}$$

with

$$d_{mn} = \sqrt{(x_m - x_n)^2 + (y_m - y_n)^2}. \tag{43}$$

The exponent of the integrand in Eq. (40) can be rewritten as

$$\begin{aligned} &(x_m - x_n)\cos(\theta+\beta) + (y_m - y_n)\sin(\theta+\beta) \\ &\quad = d_{mn}\left[\cos(\beta)\cos(\theta+\beta) + \sin(\beta)\sin(\theta+\beta)\right] \\ &\quad = d_{mn}\cos(\theta), \end{aligned} \tag{44}$$

which simplifies Eq. (40) to

$$J(\vec{x_1}, \cdots, \vec{x_N}) = \frac{1}{N^2}\sum_{m=1}^{N}\sum_{n=1}^{N}\int_{\phi_{min}}^{\phi_{max}} k^2\cos(\phi)\sin(\phi)\int_0^{2\pi} \mathrm{e}^{-ik\sin(\phi)d_{mn}\cos(\theta)}\mathrm{d}\theta\mathrm{d}\phi. \tag{45}$$

The inner integral over θ can be written as

$$\int_0^{2\pi} \mathrm{e}^{-ik\sin(\phi)d_{mn}\cos(\theta)}\mathrm{d}\theta = \int_0^{2\pi} \cos\left[-k\sin(\phi)d_{mn}\cos(\theta)\right]\mathrm{d}\theta + i\int_0^{2\pi} \sin\left[k\sin(\phi)d_{mn}\cos(\theta)\right]\mathrm{d}\theta, \tag{46}$$

where the integrand of the imaginary part is an odd function with period 2π which results in the integral being zero. For the integral containing the cosine, it can be graphically seen as the

integrand to be a periodic function with frequency 2θ. This results in

$$\int_0^{2\pi} \mathrm{e}^{-ik\sin(\phi)d_{mn}\cos(\theta)}\mathrm{d}\theta = 2\int_0^{\pi} \cos\left[k\sin(\phi)d_{mn}\cos(\theta)\right]\mathrm{d}\theta \tag{47}$$

The integral on the right-hand side of Eq. (47) is known as the Bessel function of the first kind with zero order, i.e. $\int_0^{\pi}\cos\left(k\sin(\phi)d_{mn}\cos(\theta)\right)\mathrm{d}\theta = \pi J_0(k\sin(\phi)d_{mn})$. Using the Bessel function we can write the objective function as

$$J(\vec{x_1},\cdots,\vec{x_N}) = \frac{2\pi}{N^2}\sum_{m=1}^{N}\sum_{n=1}^{N}\int_{\phi_{min}}^{\phi_{max}} k^2\cos(\phi)\sin(\phi)J_0\left(k\sin(\phi)d_{mn}\right)\mathrm{d}\phi. \tag{48}$$

For the case $m=n$, $d_{mn}=0$ so $J_0(0)=1$. Using this given information we can split up the summation as

$$J(\vec{x_1},\cdots,\vec{x_N}) = \frac{\pi}{N^2}\left[\sum_{n=1}^{N}\int_{\phi_{min}}^{\phi_{max}} 2k^2\cos(\phi)\sin(\phi)\mathrm{d}\phi + 2\sum_{m=1}^{N}\sum_{\substack{n=1\\n\neq m}}^{N}\int_{\phi_{min}}^{\phi_{max}} k^2\cos(\phi)\sin(\phi)J_0\left(k\sin(\phi)d_{mn}\right)\mathrm{d}\phi\right]. \tag{49}$$

Using $\mathrm{d}(\sin^2\phi) = 2\cos(\phi)\sin(\phi)\mathrm{d}\phi$ the first part on the right-hand side is

$$\sum_{n=1}^{N}\int_{\phi_{min}}^{\phi_{max}} k^2\mathrm{d}(\sin^2\phi) = \sum_{n=1}^{N}\left[k^2\sin^2\phi\right]_{\phi_{min}}^{\phi_{max}} = Nk^2\left[\sin^2(\phi_{max})-\sin^2(\phi_{min})\right]. \tag{50}$$

The second part can be solved using the substitution $u = k\sin(\phi)d_{mn}, \mathrm{d}u = k\cos(\phi)d_{mn}\mathrm{d}\phi$ to get

$$\int_{\phi_{min}}^{\phi_{max}} k^2\cos(\phi)\sin(\phi)J_0\left(k\sin(\phi)d_{mn}\right)\mathrm{d}\phi = \frac{1}{d_{mn}^2}\int_{k\sin(\phi_{min})d_{mn}}^{k\sin(\phi_{max})d_{mn}} uJ_0\left(u\right)\mathrm{d}u, \tag{51}$$

which can be related to the derivative of $J_1(u)$ as[19]

$$\begin{aligned}\int_{k\sin(\phi_{min})d_{mn}}^{k\sin(\phi_{max})d_{mn}} uJ_0\left(u\right)\mathrm{d}u &= \int_{k\sin(\phi_{min})d_{mn}}^{k\sin(\phi_{max})d_{mn}} \frac{\mathrm{d}}{\mathrm{d}u}\left[uJ_1(u)\right]\mathrm{d}u \\ &= k\sin(\phi_{max})d_{mn}J_1[k\sin(\phi_{max})d_{mn}] - k\sin(\phi_{min})d_{mn}J_1[k\sin(\phi_{min})d_{mn}]\end{aligned}. \tag{52}$$

Using Eq. (50), Eq. (51) and Eq. (52) in Eq. (49) and the fact $d_{mn} = d_{nm}$ we get for the

objective function

$$J(\vec{x_1},\cdots,\vec{x_N}) = \frac{\pi k}{N^2}\left(Nk\left[\sin^2(\phi_{max})-\sin^2(\phi_{min})\right]\right. \\ \left. +4\sum_{m=1}^{N-1}\sum_{n=m+1}^{N}\frac{\sin(\phi_{max})J_1[k\sin(\phi_{max})d_{mn}]-\sin(\phi_{min})J_1[k\sin(\phi_{min})d_{mn}]}{d_{mn}}\right), \tag{53}$$

where we notice the summation boundary changed reducing the amount of calculations for J by half.